CORE
Metadata, citation and similar papers at core.ac.uk
Provided by NRC Publications Archive

NRC Publications Archive (NPArC)
Archives des publications du CNRC (NPArC)

**Optical Coherence Tomography for the Inspection of Plasma-Sprayed Ceramic Coatings**

Veilleux, J.; Boulos, M.; Moreau, C.; Lévesque, D.; Dufour, M.

**Publisher's version / la version de l'éditeur:**
*Thermal Spray 2006: Science, Innovation, and Application, pp. 1077-1082, 2006*

**Web page / page Web**

http://nparc.cisti-icist.nrc-cnrc.gc.ca/npsi/ctrl?action=rtdoc&an=15877983&lang=en
http://nparc.cisti-icist.nrc-cnrc.gc.ca/npsi/ctrl?action=rtdoc&an=15877983&lang=fr

Access and use of this website and the material on it are subject to the Terms and Conditions set forth at
http://nparc.cisti-icist.nrc-cnrc.gc.ca/npsi/jsp/nparc_cp.jsp?lang=en
READ THESE TERMS AND CONDITIONS CAREFULLY BEFORE USING THIS WEBSITE.

L'accès à ce site Web et l'utilisation de son contenu sont assujettis aux conditions présentées dans le site
http://nparc.cisti-icist.nrc-cnrc.gc.ca/npsi/jsp/nparc_cp.jsp?lang=fr
LISEZ CES CONDITIONS ATTENTIVEMENT AVANT D'UTILISER CE SITE WEB.

Contact us / Contactez nous: nparc.cisti@nrc-cnrc.gc.ca.

National Research Council Canada
Conseil national de recherches Canada
Canada

imi 2006-112600-9
CNRC 48861

# Optical Coherence Tomography for the Inspection of Plasma-Sprayed Ceramic Coatings

*J. Veilleux, M. Boulos*
*Department of Chemical Engineering, University of Sherbrooke, Sherbrooke, Québec, Canada*

*C. Moreau, D. Lévesque, M. Dufour*
*Industrial Materials Institute, National Research Council Canada, Boucherville, Québec, Canada*

**Abstract**

Optical coherence tomography (OCT) is evaluated as a promising technique for microstructure characterization of plasma-sprayed ceramic coatings. OCT combines the principles of low coherence interferometry and optical heterodyne detection to obtain both a high sensitivity to weakly backscattered light and a high axial resolution. It can be used to accurately locate interfaces where the refractive index changes abruptly within translucent materials. In the present work, OCT cross-sectional images of thin yttria-stabilized zirconia (YSZ) coatings are considered. The interferograms forming the images are analyzed individually to successfully gather information related to light penetration depth inside coatings. The interferogram analysis allows the evaluation of the refractive index of the YSZ non-transformable tetragonal phase.

## Introduction

It is now well established that plasma-sprayed ceramic coatings are appreciably contributing to the reduction of premature material degradation in harsh environment [1]. For example, they act as thermal barrier and protective coatings against wear and corrosion in the aeronautical [2] and automotive [3] industries. As well, they are used as biocompatible coatings deposited on biomedical implants [4]. In many of these applications currently in development, the quality of plasma-sprayed ceramic coatings is critical not only to protect the coated part, but also to ensure its proper and safe use to avoid catastrophic failure. However, plasma spraying is a stochastic process through which the feedstock ceramic particles are melted and accelerated to impinge the substrate where they rapidly solidify and form splats. The resulting microstructure of this random coating build-up is characterized by the existence of interlamellar pores, globular pores and splat interfaces which are known to significantly influence coatings thermal conductivity and mechanical properties [5]. Therefore, a close control of the coating microstructure is sought to meet the requirements of the coated part application. It thus becomes imperative to develop a non-destructive evaluation (NDE) technique to observe and characterize the microstructure (and especially the porosity) of plasma-sprayed ceramic coatings.

In this regard, optical coherence tomography (OCT), a NDE technology that was predominantly developed for cross-sectional imaging of biological systems microstructure [6], has some promising features. In fact, OCT presents an axial resolution compatible with large splats optical thickness as well as a good sensitivity to ceramic/air interfaces. In particular, OCT is expected to be sensitive to interlamellar contact and to globular porosity. Although briefly discuss by Moreau [7], the use of OCT to characterize plasma-sprayed thermal barrier coatings has not been extensively explored. However, some interesting studies illustrate OCT inspection performances by describing its capability to detect subsurface defects in $Si_3N_4$ ceramic balls [8] and to image polymer matrix composites [9].

In the present work, OCT interferograms of four different yttria-stabilized zirconia (YSZ) coatings are collected and analyzed to evaluate an average light penetration depth inside the coatings. Some preliminary results show that this average penetration depth varies with overall porosity percentage and with feedstock powder distribution. In an other set of experiments, the interferogram analysis also allows the evaluation of the refractive index of YSZ non-transformable tetragonal phase.

## Principles of OCT

As shown in Fig. 1, an OCT system is actually based on a Michelson interferometer. The light emitted by a broadband

source (superluminescent diode – SLD) is divided at a beam splitter (BS) into two distinct optical paths that are respectively oriented towards the reference mirror and the sample. When the light returns, if the optical path length mismatch between reference and sample arms is shorter than the light coherence length, both the sample backscattered field and the reference field will combine to produce an interference signal (or interferogram) collected by the photodetector, amplified and digitally processed (filtered and demodulated). By recording this interference signal as the reference mirror is synchronously translated, the axial profile of the sample backscattering properties can be obtained. The axial resolution in this profile depends on the coherence length of the light source. Consequently, a high resolution can be achieved independently of the beam focusing conditions, thus of the sample arm optics. In fact, for a light source with a Gaussian spectral distribution, it can be shown [10] that the axial resolution $\Delta z$ of the OCT system is inversely proportional to the bandwidth $\Delta\lambda$ of the power spectrum centered at a wavelength $\lambda$:

$$\Delta z = \left(\frac{2\ln 2}{\pi}\right)\left(\frac{\lambda^2}{\Delta\lambda}\right). \quad (1)$$

## Experimental Procedure

Plasma Spraying

Four different YSZ coatings were sprayed on grit-blasted steel substrate using a Sulzer Metco F4-MB plasma torch, which uses external radial powder injection and swirl flow gas injection. Argon (primary gas flow rate of 35.0 slm) and hydrogen (secondary gas flow rate of 12.0 slm) were used as the plasma gas mixture. The power input was held to 28 or 35 kW, with power variations being obtained through current

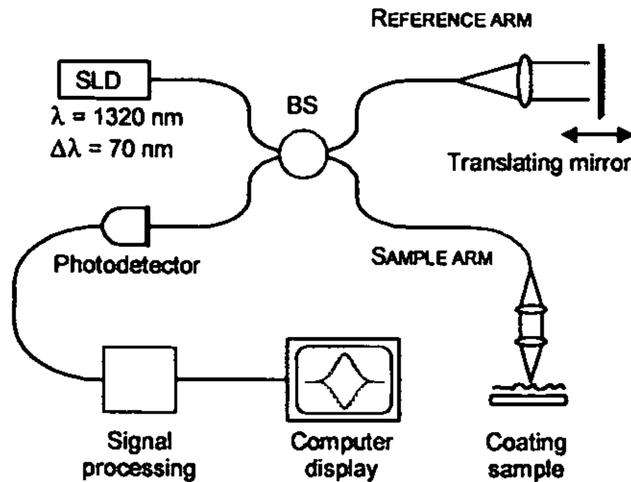


*Figure 1: Schematic representation of the OCT system based on a Michelson interferometer used in the present work.*

*Table 1: Variations of experimental spraying conditions, thickness and porosity of the four samples. In the sample ID column, H and L stand respectively for high and low power.*

| Sample ID | Powder | Power (kW) | Coating thickness (μm) | Porosity (%) |
|---|---|---|---|---|
| 825.1-H | 825.1 | 35 | 115 ± 6 | 4.6 ± 0.7 |
| 825.1-L | 825.1 | 28 | 157 ± 9 | 7.8 ± 0.6 |
| 825.0-H | 825.0 | 35 | 100 ± 7 | 5.3 ± 0.5 |
| 825.0-L | 825.0 | 28 | 152 ± 7 | 8.6 ± 0.6 |

increases from 425 to 550 A. The YSZ feedstock powders selected, H.C. Starck Amperit 825.0 (22/5 $\mu$m) and 825.1 (45/22 $\mu$m), were injected at a feed rate of 25 g/min with argon as carrier gas (3 slm). Table 1 shows in details the varying spray conditions for the four YSZ coatings deposited. In each case, plasma torch stand off distance was kept constant at 120 mm. Finally, during spraying, the samples were continuously cooled down with an air jet to maintain the surface temperature between 175°C and 225°C.

Coating thickness and porosity were both determined by image analysis of the SEM micrographies (JEOL JSM-6100) shown in Fig. 2. The values given in Table 1 correspond to an average of ten measurements for which an uncertainty of one standard deviation is also given. A field-emission gun SEM (Hitachi S-4700) was used to characterize coating splat microstructure. An example is shown in Fig. 3 for a fracture of samples 825.1-H and 825.0-H.

As expected, the coatings built under higher plasma torch power present a lower porosity level (4.6% and 5.3% vs 7.8% and 8.6%). Moreover, the larger powder produces thicker splats as it can be seen in Fig. 3. In fact, splats of 8 μm are observed in Fig. 3a whereas splats in Fig. 3b have a maximum thickness of 5 μm. These differences are expected to significantly affect the interferograms collected by OCT. In particular, different interlamellar pores and splat interfaces should influence light attenuation.

Optical Coherence Tomography

The coatings were then imaged with the OCT system shown in Fig. 1. Unless otherwise stated, YSZ coatings were observed as sprayed, without any special preparation. The optical source coupled into the interferometer was a Covega SLED emitting over a 70 nm wide bandwidth centered at a wavelength of 1320 nm. Thus, the system axial resolution (calculated from Eq. 1) is 11 $\mu$m. The maximum emitted power was 17 mW from which only 10% was actually coupled into the interferometer to avoid saturation of the photodetector. In the sample arm, a 2.4-mm wide collimated beam was focused onto the sample coating surface using a lens with a focal length of 25 mm. Therefore, the resulting transverse resolution of the system is 18 $\mu$m.

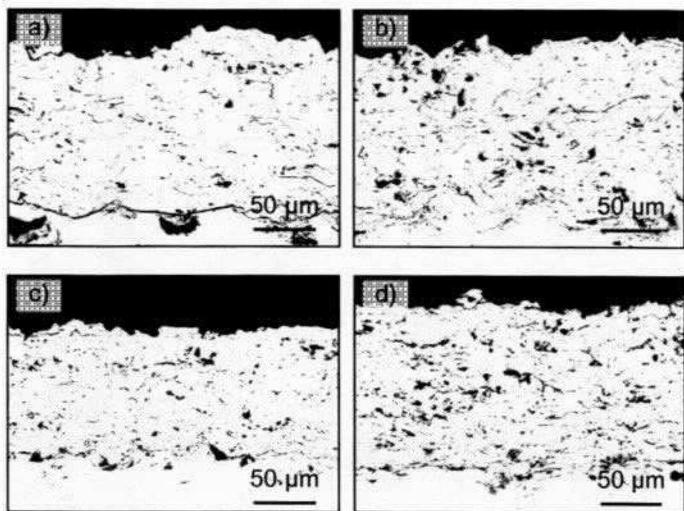


*Figure 2: SEM micrographies showing the different levels of porosity for the coating samples a) 825.1-H, b) 825.1-L, c) 825.0-H and d) 825.0-L.*

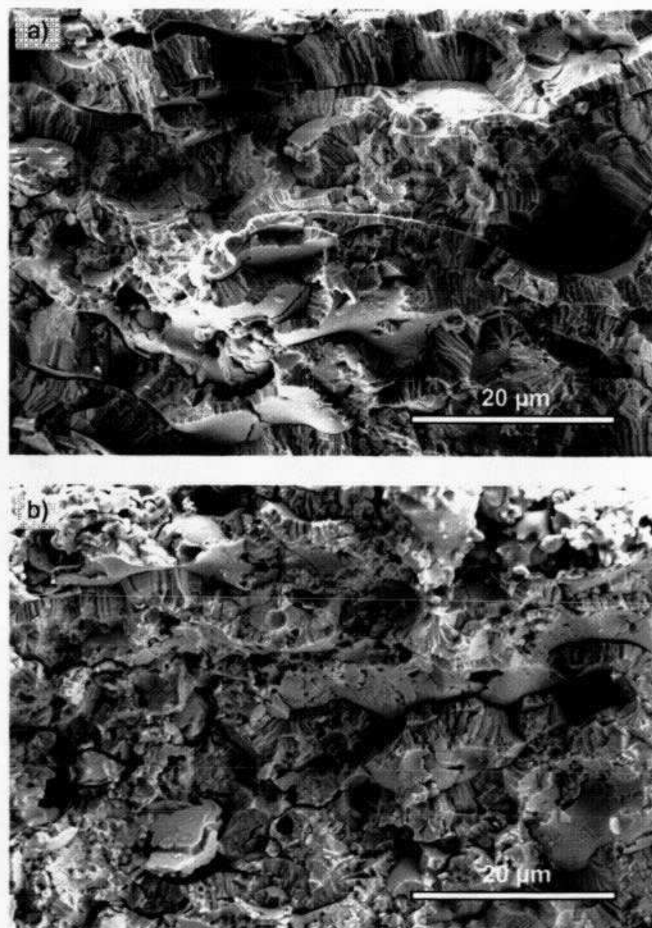


*Figure 3: SEM fractographies showing splat microstructure of samples a) 825.1-H and b) 825.0-H.*

For each coating sample, 250 interferograms were collected to form a single cross-sectional image and the procedure was repeated 10 times. The step size between two successive interferograms was 25 $\mu$m, and the separation between two cross-sectional images was 25 $\mu$m. Thus, 10 cross-sectional images with dimensions of 6.25 mm wide and 2.35 mm deep were collected for each sample.

## Results and Discussion

### Light Penetration Depth

Cross-sectional imaging of YSZ coatings was performed and images are shown in Fig. 4. Even if the coatings are relatively thin, the coating/substrate interface cannot be identified. Peaks coming from this interface are most probably lost among multiple scattering events. Some areas (especially for samples 825.0-H and 825.0-L) show higher light attenuation (blueish columns), possibly revealing the presence of defects (porosity, inclusion, etc.). On-going experiments are led to explain this attenuation phenomenon. Besides these observations, light penetration (which can be observed by the transition from red to blue) seems quite similar for the four coatings. However, statistically significant differences exist between samples, as discussed below.

The mean light penetration depth inside coatings is evaluated to provide an approximative indication of light attenuation. This attenuation results from scattering and absorption events that occur along the optical path and therefore depends on coating microstructure. Since YSZ absorption at $\lambda = 1.32$ $\mu$m is relatively small (when compared to scattering) and because forward scattering is important, the general Beer-Lambert law of attenuation could not be directly applied to retrieve light penetration depth. Moreover, it requires a time consuming algorithm to identify interferogram peaks that are needed to fit a straight line (on a logarithmic scale) and to determine its slope from which light penetration depth can be evaluated. For these reasons, a different approach was chosen to estimate light attenuation.

As a simple statistical measure of light penetration depth inside coatings, an average value of the interferogram amplitude center position or centroid (by analogy to a mass center) was calculated by taking the mean amplitude center position over 250 interferograms:

$$Average\ centroid = \frac{1}{250}\sum_i \left( \frac{\sum_j Position_j \times Ampl_{ij}}{\sum_j Ampl_{ij}} \right). \quad (2)$$

In the equation, the subscript $i$ refers to the $i^{th}$ interferogram of the cross-sectional image, while $j$ stands for the $j^{th}$ position in this interferogram. This average centroid is taken as an effective and reliable estimate of light penetration depth. In

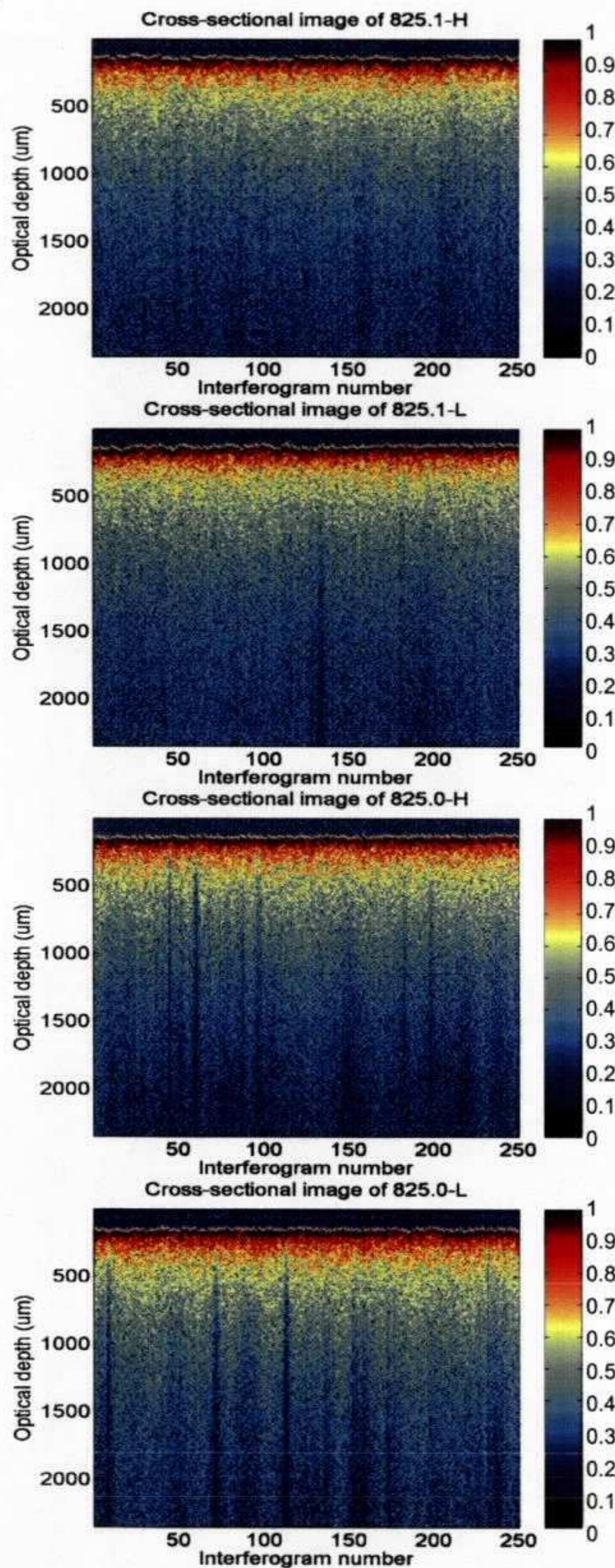


*Figure 4: OCT cross-sectional images of the four samples showing normalized logarithmic amplitude as a function of optical depth for 250 interferograms separated by a step size of 25 μm.*

fact, fluctuations in individual centroid of the interferograms along a cross-sectional image are relatively small (results not shown). Furthermore, variations of this parameter between cross-sectional images taken from one sample are small, as shown in Fig. 5a.

Figure 5b shows the significant differences between average centroid for the four YSZ coatings. The following two observations can be drawn. First, without considering porosity, light penetration depth is larger for the larger powder (Amperit 825.1). Second, with same powder size, light penetration depth is larger in coatings produced at lower torch power (L). Both factors can be justified by the number of air/ceramic interfaces crossed by the sample beam along its optical path. In fact, since each crossed interface scatters light, the higher their number the lower the penetration depth. Therefore, knowing that the number of interfaces per unit length is larger for the coating made with the smaller powder (Amperit 825.0), one can justify its higher attenuation when compared to coatings made with Amperit 825.1. On the other hand, coatings produced at lower torch power are more porous (as determined by SEM image analysis) and have fewer interfaces from which light can be scattered. In fact, when the light beam penetrates a globular or an interlamellar pore, no

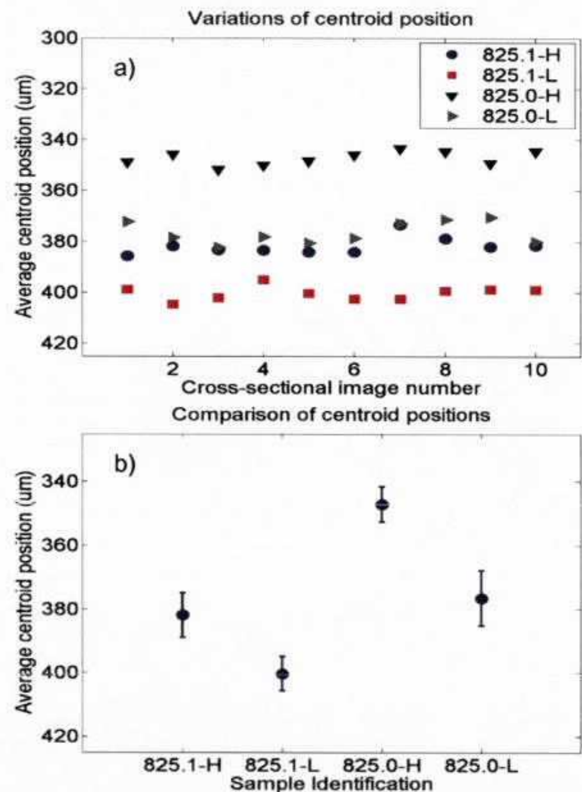


*Figure 5: a) Limited variations of the average centroid position for 10 cross-sectional images of the four YSZ coatings. b) Comparison of the average centroid position (calculated from Fig. 5a) for the coating samples.*

scattering occurs until it reaches the splat located at the bottom of the pore. In addition, fewer interfaces are found in 825.0-L and 825.1-L since average lamella thickness is larger (owing to uncompletely melted particles) when the torch power is decreased. Further work will involved a larger number of samples (4 powder distributions and 4 porosity levels) to corroborate these arguments.

Absorption is another factor that should contribute to light attenuation inside YSZ coatings. As shown by Debout et al. [11], the oxygen loss that occurs in YSZ during the deposition process (which results in darker coatings) increases significantly light absorption in the near IR range. In our analysis, YSZ absorption was neglected in a first approximation, but an evaluation of its impact on OCT interferograms will be performed by annealing the coatings in further experiments.

YSZ Refractive Index

The evaluation of the index of refraction requires a few extra steps for sample preparation, which are described here. A YSZ coating was deposited under the spraying conditions depicted earlier, but with a slightly increased overspray cooling to maintain the surface temperature around 125°C. The powder and power chosen were respectively Amperit 825.1 and 28 kW. The resulting coating, identified 825.1-L2, has a thickness of 235 ± 11 $\mu$m and a porosity of 10.0 ± 2.0 %. The coating was detached from its steel substrate by acid dissolution and polished on both sides to form a wedge. Afterward, it was placed over a silicon wafer (Fig. 6) which provides two parallel reference surfaces for subsequent OCT cross-sectional imaging. Silicon was chosen for its high refractive index and its very low attenuation at the selected wavelength. The OCT scanning parameters were slightly changed as compared to those of the previous images: a single cross-sectional image of dimensions 10 mm wide and 3 mm deep, formed by 1000 interferograms (step size of 10 μm), was collected.

The resulting cross-sectional image is shown in Fig. 7a. As in previous images, the coating/Si interface cannot be identified, possibly due to multiple scattering events. However, the Si back surface with an amplitude decreasing with coating thickness can be clearly observed. Since the Si wafer has very low attenuation, the back surface detection limit depends on the coating only. Also, this OCT image was used to identify

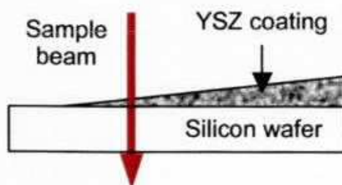


*Figure 6 : Schematic representation of the YSZ coating wedge placed over a silicon wafer.*

two representative interferograms to evaluate the index of refraction of the coating. The first one was selected from a zone where the sample beam impinges only on the reference Si wafer, and the second one was extracted at a location where the sample beam gets through both the YSZ coating and the Si wafer (e.g. at the Si back surface detection limit). The corresponding interferograms are shown in Fig. 7b and Fig. 7c. Dashed lines are plotted to appreciate the peak position shifts in optical depth at the coating top surface and at the Si wafer bottom surface. Therefore, the geometric coating

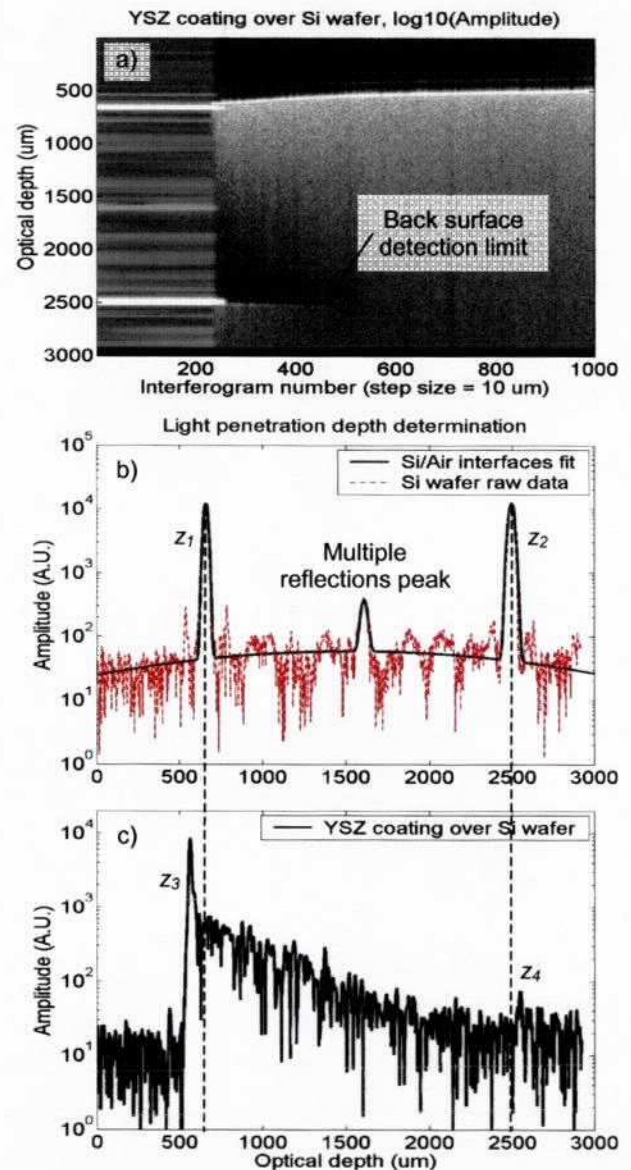


*Figure 7: a) OCT cross-sectional image of a YSZ coating placed over a silicon wafer. b) Silicon wafer reference interfaces (interferogram #5 in Fig. 7a). c) Surface shifts observed when the beam crosses both the YSZ coating and the Si wafer (interferogram #445 in Fig. 7a).*

thickness is given by the simple profilometry difference $z_1 - z_3$ and the back surface shift (involving the coating refractive index and thickness) is given by $z_4 - z_2$. Obviously, there should be an equivalent back shift for the Si wafer top surface peak position when light gets through the coating, but this peak is undetectable. Knowing that the coating contains about 10% porosity, the index of refraction $n_{YSZ}$ of YSZ non-transformable tetragonal phase (which refers to a stable form of the tetragonal phase resulting from plasma spraying [12]) can be extracted from:

$$[(0.9\, n_{YSZ} + 0.1\, n_{air}) - 1]e = d \,. \quad (3)$$

where $n_{air}$ is the air refractive index, $e = z_1 - z_3$ is the coating thickness and $d = z_4 - z_2$ is the Si wafer back surface shift. Thus, measuring in Fig. 7 a coating thickness $e = 96 \pm 5$ $\mu$m and a back surface shift $d = 55 \pm 5$ $\mu$m, the index of refraction of YSZ non-transformable tetragonal phase is evaluated as $n_{YSZ} = 1.64 \pm 0.1$. To the authors' knowledge, this is the first evaluation of the refractive index of YSZ non-transformable tetragonal phase. In comparison to the reported refractive index of about 2.1 for YSZ cubic phase [13], the value found seems quite small. However, the phase transition from cubic to tetragonal of pure evaporated zirconia (which comes with a few percent increase in volume) has been found to influence significantly the refractive index, bringing it down to a value close to 1.7 [14]. The same behavior apparently affects plasma-sprayed YSZ.

## Conclusion

Different plasma spraying conditions were applied to deposit YSZ coatings. Their thickness and porosity were evaluated by SEM image analysis and OCT cross-sectional imaging was performed. An estimate of light penetration depth was calculated by an average amplitude center or centroid for each sample. It was found that powder size and porosity affect light penetration depth. In fact, light penetrates deeper in the coating made with larger powder and having a higher porosity level. These observations can be explained by a reduced number of air/ceramic interfaces (which represent scattering sites for light) in such a coating. In further work, additional YSZ samples (with larger variations in porosity level and powder size distribution) will be plasma-sprayed and imaged by OCT to corroborate these arguments. Other OCT experiments, processing and analysis of the interferograms will also be investigated. For example, one experiment will try to correlate high attenuation zone in a cross-section with the presence of real defects inside the coating. Furthermore, deconvolution algorithms (Wiener filtering, CLEAN algorithm) will be applied to improve axial resolution and thus hopefully resolve splat interfaces.

In another experiment, a plasma-sprayed YSZ coating wedge was placed onto a reference silicon wafer and its OCT cross-sectional image was used to evaluate the refractive index of the YSZ non-transformable tetragonal phase. From the observed peak shifts, an index of refraction of 1.64 ± 0.1 was found.

## Acknowledgments

The financial support by the Natural Sciences and Engineering Research Council of Canada (NSERC), the National Research Council Canada (NRC), and the Fonds Québécois de la Recherche sur la Nature et les Technologies (FQRNT), is gratefully acknowledged. The authors also appreciate helpful technical support of Bruno Gauthier and fruitful discussions with Guy Lamouche.

## References

1. X. Q. Cao, R. Vassen and D. Stoever, *J. Eur. Ceram. Soc.*, Vol 24 (No. 1), 2004, p 1-10
2. J. R. Nicholls, *MRS Bulletin*, Vol 28 (No. 9), 2003, p 659-670
3. N. B. Dahotre and S. Nayak, *Surface and Coatings Technology*, Vol 194 (No. 1), 2005, p 58-67
4. L. Sun, C. C. Berndt, K. A. Gross and A. Kucuk, *J. Biomed. Mater. Res. B: Appl. Biomater.*, Vol 58 (No. 5), 2001, p 570-592
5. Z. Wang, A. Kulkarni, S. Deshpande and coll., *Acta Materialia*, Vol 51 (No. 18), 2003, p 5319-5334
6. D. Huang, E. A. Swanson, C. P. Lin and coll., *Science*, Vol 254 (No. 5035), 1991, p 1178-1181
7. C. Moreau, Towards a better control of thermal spray processes, *Thermal spray – Meeting the Challenges of the 21st Century*, C. Coddet, Ed., May 25-29, 1998 (Nice, France), ASM International, 1998, p 1681-1693
8. M. Bashkansky, D. Lewis III, V. Pujari and coll., *NDT&E International*, Vol 34 (No. 8), 2001, p 547-555
9. J. P. Dunkers, F. R. Phelan, D. P. Sanders and coll., *Optics and Lasers in Engineering*, Vol 35 (No. 3), 2001, p 135-147
10. M. R. Hee, Optical Coherence Tomography: Theory, *Handbook of Optical Coherence Tomography*, B. E. Bouma and G. J. Tearney, Eds., New York, Marcel Dekker, 2002, p 41-66
11. V. Debout, E. Bruneton, E. Meillot and coll., Correlation between processing parameters, microstructure and optical properties for plasma-sprayed yttria-stabilized zirconia coatings, *17th International Symposium on Plasma Chemistry Proceedings*, August 7-12, 2005 (Toronto, Canada), IPCS, 2005
12. P. Scardi, M. Leoni and L. Bertamini, *Surface and Coatings Technology*, Vol 76-77, 1995, p 106-112
13. D. L. Wood, K. Nassau and T. Y. Kometani, *Applied Optics*, Vol 29 (No. 16), 1990, p 2485-2488
14. M. G. Krishna, K. N. Rao and S. Mohan, *Appl. Phys. Lett.*, Vol 57 (No. 6), 1990, p 557-559